Plastic deformation of dense nanocrystalline yttrium oxide at elevated temperatures

Angela Gallardo-López [a,*], Arturo Domínguez-Rodríguez [a], Claude Estournès [b], Rachel Marder [c], Rachman Chaim [c]

[a] *Departmento de Fisica de la Materia Condensada, Universidad de Sevilla, 41012 Sevilla, Spain*
[b] *CNRS, Institute Carnot Cirimat, F-31602 Toulouse Cedex 9, France*
[c] *Department of Materials Engineering, Technion – Israel Institute of Technology, Haifa 32000, Israel*

Abstract

Nanocrystalline yttrium oxide, Y_2O_3 with 110 nm average grain size was plastically deformed between 800 °C and 1100 °C by compression at different strain rates and by creep at different stresses. The onset temperature for plasticity was at 1000 °C. Yield stress was strongly temperature dependent and the strain hardening disappeared at 1100 °C. The polyhedral and equiaxed grain morphology were preserved in the deformed specimens. The experimentally measured and theoretically calculated stress exponent $n = 2$ was consistent with the plastic deformation by grain boundary sliding. Decrease in the grain size was consistent with decrease in the brittle to ductile transition temperature.

Keywords: B. Electron microscopy; C. Plasticity; C. Grain boundary sliding; D. Yttrium oxide

1. Introduction

Characterization of the plastic deformation and the respective deformation mechanisms in nano-materials is basic for predicting their behavior for structural applications at elevated temperatures. These data are also beneficial for tailoring the nanostructure for the enhanced plasticity. In the last two decades, efforts have been directed to decrease the grain size of ceramics to improve their strength and fracture toughness at room and high temperatures. The expected effect of the nanometric grain size on the low temperature plasticity and superplasticity of ceramics have led to extensive efforts to fabricate fully dense nanocrystalline ceramics. However, the grain size–density trajectory is in jeopardy with the preservation of the nanocrystalline character in the fully-dense ceramics, fabricated by conventional techniques. Recently, the novel technique of spark plasma sintering (SPS) has been used for rapid fabrication of fully dense nanostructure oxides.[1–4]

Different monolithic nanocrystalline and nano-composite ceramics have been examined for their plastic and superplastic behavior.[5–10] However, high strain rates up to $10^{-1}\,s^{-1}$ were reported only at high homologous temperatures, i.e. $0.65\,T_m$, where T_m is the ceramic melting temperature.[5,6] The well-known tetragonal zirconia alloy (Y-TZP) or its pure nanocrystalline monoclinic version,[7,8] as well as soft nanocrystalline MgO,[9] did not reveal high strain rate plasticity at low homologous temperature. Albeit the superplastic behavior in ultrafine ceramics has been related to the grain boundary sliding mechanism, the actual deformation mechanism is still under debate and may be material dependent.[10–12] Recently new plastic deformation mechanisms by non-local homogeneous nucleation of nano-scale loop of partial dislocations,[13] and unusual nonlinear stress and grain size dependence,[14] were assumed to facilitate the nanocrystalline plasticity.

Yttrium oxide is an important high melting point oxide (2450 °C) used both as functional and structural ceramic hence its plastic deformation behavior is of a prime importance for its fabrication and usage at the elevated temperatures. Plastic deformation of Y_2O_3 single crystals[15–17] as well as polycrystals[18–20] with conventional grain size has been extensively investigated at high temperatures. These investigations in single crystals

* Corresponding author. Tel.: +34 95 455 4448; fax: +34 95 455 2870.
E-mail address: angela@us.es (A. Gallardo-López).

http://dx.doi.org/10.1016/j.jeurceramsoc.2012.04.035

confirmed the high temperature dislocation activity to take place by glide at high stresses and by climb at low stresses.[16] Moreover high local stresses by indentation were observed to induce plastic deformation by twinning. Superplastic-like behavior was observed in polycrystalline Y_2O_3 with ultrafine grains.[18,20] However, the only investigations exist on deformation behavior of nanocrystalline yttria arise from densification studies and due to the lack of appropriate fully dense specimens. Nevertheless, recently dense nanocrystalline Y_2O_3 were successfully fabricated using spark plasma sintering.[21–23] In the present work, the plastic behavior of fully dense nanocrystalline Y_2O_3 at low homologous temperatures has been examined and reported.

2. Experimental

Ultrapure nanocrystalline Y_2O_3 powder (99.99%, 18 nm average particle diameter, Cathay Advanced Materials, China) was used for fabrication of 98.3% dense nanocrystalline discs of 8 mm diameter and 2 mm thickness. The disc specimens were fabricated by spark plasma sintering at 1100 °C and 100 MPa for 20 min, using the heating rate of 180 °C min^{-1}; this resulted in 110 nm average grain size (diameter) and 18 nm average pore size, located at the grain corners. The fabrication and the sintered material characteristics were described in detail elsewhere.[22] Rectangular bars of 2 mm × 2 mm × 3.5 mm were cut from the discs using a diamond saw and then grinded with a discoplan to assure parallelism of all opposite faces. The bar length was perpendicular to the compression axis in the SPS process. The bars were uni-axially compressed along their length at two different regimes. The first set of specimens was deformed at constant crosshead speed (herein *constant strain-rate regime*) in an Instron machine (model 1185) using SiC rams. Each specimen was placed between the rams, heated in the furnace enclosing the ensemble and deformed while one of the rams approaches the opposite at a constant speed which was set externally. The second set of the specimens was deformed at constant load (herein *constant stress/creep regime*). The creep tests were performed using a prototype machine designed for the compression tests using alumina rams as described in detail elsewhere.[24] The applied stresses ranged from 90 to 390 MPa and the strain rates varied between 5×10^{-7} and 3×10^{-5} s^{-1}. Most of the compression tests were performed in the temperature range 1050–1100 °C where grain growth was insignificant[22] and yet the plastic behavior was observed. Most compression tests were performed in air, although for some creep experiments, as indicated, an inert Ar atmosphere was used to check for differences in the plastic behavior, though no difference was found, as stated by previous works.[25] Due to the shortage in specimens no reference specimens were used for static grain growth studies.

Selected deformed specimens from both test regimes (constant strain rate and creep) together with the as-received reference specimen were used for the microstructure characterization by scanning (E-SEM Quanta 200, operated at 25 kV) and transmission (TEM, Tecnai G^2 T20, operated at 200 kV) electron microscopes. Appropriate foils were cut by focused ion beam (FIB) which were further thinned to electron perforation using precision ion beam polishing system (PIPS, Argon) at 5 kV. The average grain size was determined by direct measuring of the largest diameter of the polyhedral grains from several TEM images for a given specimen, counting at least 120 grains.

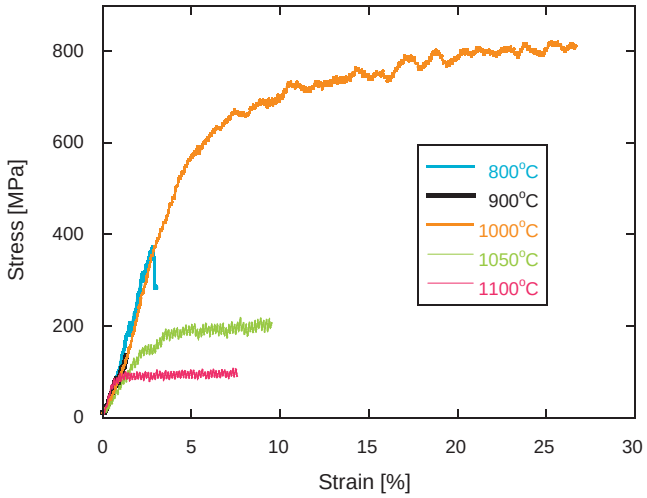

Fig. 1. Stress versus strain curves of the nanocrystalline yttria specimens deformed in compression between 800 °C and 1100 °C in air at constant strain rate (5×10^{-6} s^{-1}). Brittle failure occurred at 800 °C and 900 °C. The rest of the tests were stopped before failure. Plastic deformation is easily attained at 1000 °C.

3. Results

Plastic deformation of the nanocrystalline yttria specimens by constant strain rate occurred between 900 °C and 1000 °C (Fig. 1). Tests performed at 800 °C and 900 °C resulted in early brittle failure, but at 1000 °C a yield stress of 660 ± 10 MPa was recorded with a strain rate $\dot{\varepsilon} \approx 5 \times 10^{-6}$ s^{-1}; engineering strains higher than 35% were recorded. The yield stress drastically decreased to 160 ± 10 MPa and 90 ± 8 MPa at 1050 °C and 1100 °C, respectively. In addition, increase from 1000 °C to 1100 °C resulted in disappearance of the strain hardening during the plastic deformation; the stress–strain curve at 1100 °C may resemble that of the elastic–ideal plastic material behavior.

Deformation at the temperature range 1050–1100 °C was thoroughly investigated since it allowed reduction of the stress needed for plastic deformation and avoided possible brittle fracture damage; yet significant grain growth is inhibited. The stress exponents, n, were determined using the constitutive creep equation to adjoining segments with steady-state strain rate at the same temperature and different applied stresses:

$$\dot{\varepsilon} = A\sigma^n \exp\left(\frac{-Q}{kT}\right) \quad (1)$$

where A is a structural parameter assumed to be constant for adjoining segments when the applied stress is suddenly changed, σ is the stress, Q is the activation energy for the rate controlling mechanism, k is the Boltzmann constant and T is the absolute temperature.

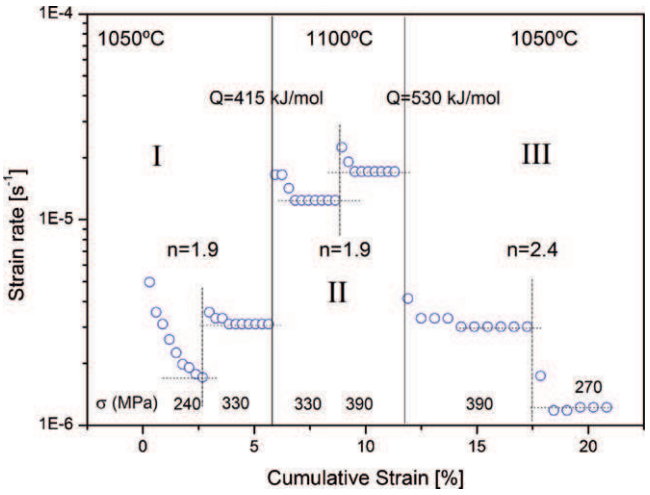

Fig. 2. Standard strain-rate versus engineering strain in constant stress interrupted creep test in Ar. The stress exponent values (n) estimated from individual stress changes and the activation energies at each temperature change were indicated. The values were calculated from the extrapolation of the quasi-stationary creep at the point of the stress or temperature change, as indicated by the dotted lines. The different temperature segments are indicated by roman numbers.

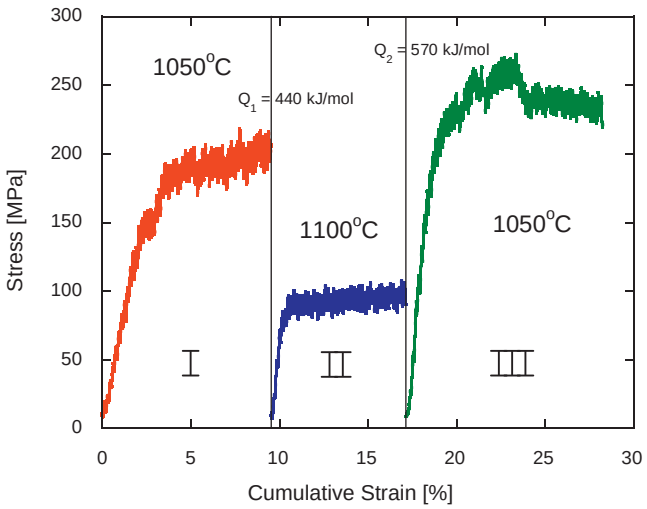

Fig. 3. Stress versus strain curves of a specimen deformed in air at constant strain-rate interrupted test with temperature changes. The values of the activation energies estimated at each temperature change were indicated. The different segments are indicated by roman numbers.

An average value of $n = 2.0 \pm 0.3$ was determined for the stress exponent via stress stepping during a set of creep experiments (for instance, segments I and III at 1050 °C in Fig. 2). This particular test was carried out in an inert argon atmosphere, although similar results were obtained in the creep tests performed in air. Stress exponents with similar values were also obtained from strain-rate changes in a set of constant strain-rate tests.

Activation energies were also determined in both creep and constant strain rate tests by temperature stepping. In this case, the constitutive creep equation (1) is used for two consecutive steady-state segments with the same stress but at different temperatures (for instance, segments I and II, at 1050 °C and 1100 °C, respectively, for creep test in Fig. 2). Several values of activation energies were obtained, from each pair of steady-state deformation segments with the same stress at different temperature, so an average value of 440 ± 70 kJ mol^{-1} was determined from a set of tests. The stress–strain plot for a specimen tested in air at constant strain rate $\sim 5 \times 10^{-6}$ s^{-1} is shown in Fig. 3. Temperature changes (three segments in Fig. 3) were performed for the same specimen in order to estimate the corresponding activation energies. The small strain hardening observed at 1050 °C disappeared when stepping up by 50 °C to 1100 °C (segment II in Fig. 3) but appeared again when the temperature was stepped down by 50–1050 °C (segment III in Fig. 3); the stress decrease in the last stage is due to the specimen degradation. Hardening was also observed in most deformation tests after a significant strain.

The nanostructure of the as-received non-deformed specimen was previously characterized.[22] It consisted of dense equiaxed polyhedral-shaped nano-grains with average diameter 110 ± 10 nm (Fig. 4). Nano-pores with 18 ± 16 nm in average diameter were also present at some grain corners and caused grain growth stagnation below 1100 °C.[22] In addition, the sintered non-deformed structure was dislocation-free except some low-angle grain boundaries between bi- or triple-grains resulting from the grain rotation. SEM images from the surface of plastically deformed specimens in air, at constant strain rate to 7% strain and with temperature changes (1050–1100–1050 °C) to 29% strain, were shown in Fig. 5. The nano-grain structure of both deformed surfaces was homogeneous but yet exhibited growth of the cavities between the nano-grains (Fig. 5a). The average grain and pore diameter in the 7% deformed specimen were 386 ± 100 nm and 123 ± 60 nm, respectively, both with log normal size distributions. Therefore, while the average grain size grew by a factor of 3, the pore diameter grew by the factor of 7. In this respect, a specimen with extended test duration, at the same strain-rate conditions but with the highest strain of 28% showed average grain size of 415 ± 96 nm together with some larger cavities developed along several connected grain boundaries and of the same order of the average grain radius (Figs. 5b and 6c).

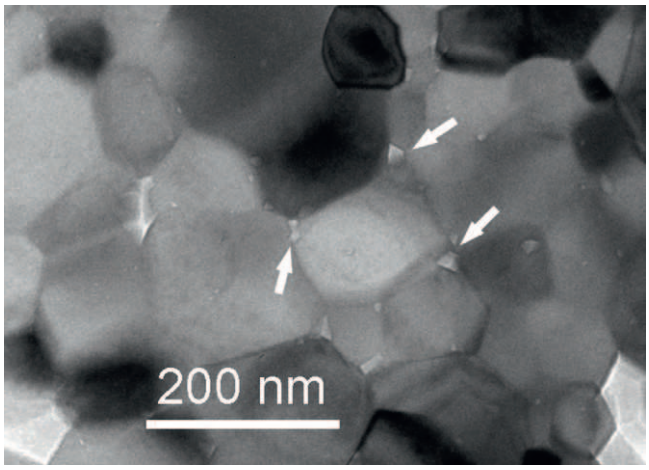

Fig. 4. TEM image showing the equiaxed polyhedral Y_2O_3 nano-grains with nano-pores at the grain corners (arrowed) in the non-deformed specimen.

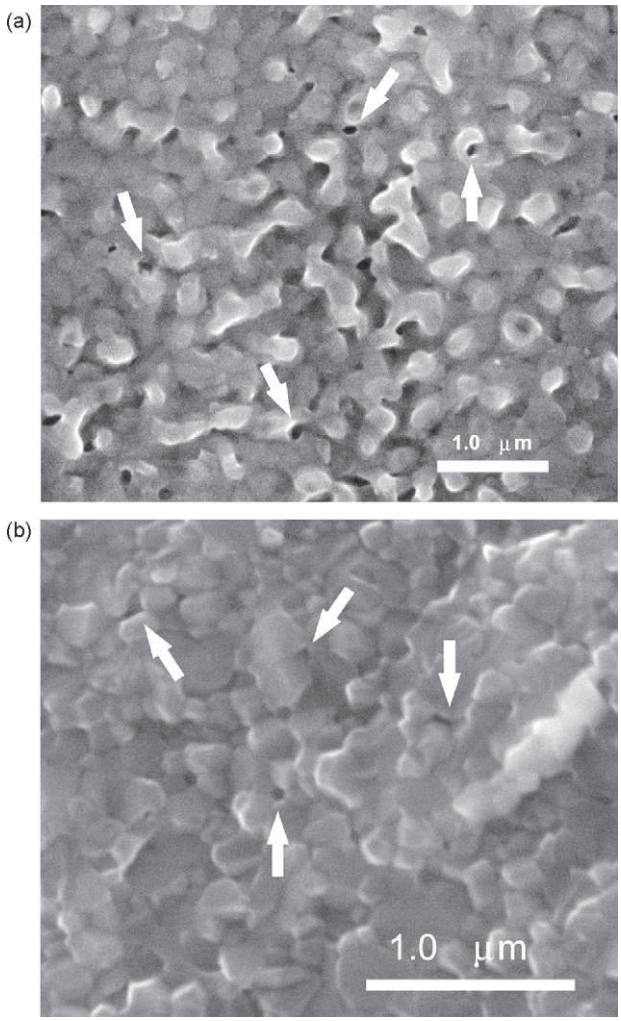

Fig. 5. SEM images from the surfaces of the nc-Y_2O_3 specimens deformed in air at constant strain-rate of $5 \times 10^{-6}\,s^{-1}$: (a) deformed at 1050 °C and 120 MPa to 7% strain. (b) Deformed with temperature changes (1050–1100–1050 °C) to 28% strain (specimen in Fig. 3). Cavities between the nano grains were arrowed.

Typical TEM images from deformed specimens by creep in Ar and at constant strain-rate in air were shown in Fig. 6. The polyhedral and equiaxed shape of the nano-grains was clearly preserved after the plastic deformation, regardless of the test type. In both specimens the former sintering cavities at the grain corners grew and in some cases extended along the grain boundaries (Fig. 6c). Tilting experiments at high magnifications confirmed the presence of some dislocations along a few especially low-angle grain boundaries, as in the as-sintered specimens. However, ultrafine dislocation loops were visible in all grains when the grain was brought into the dynamic diffracting conditions (arrowed in Fig. 6b and d). Nevertheless, the small size of these loops blurred any contrast within them needed for verification of their nature (i.e. stacking faults).

4. Discussion

As was noted above, the equiaxed morphology of the nanocrystalline grains was preserved after the plastic deformation, although some grain growth has occurred. The nano-size pores present at the grain corners in the as-sintered specimens were developed, and in some cases extended along the grain boundaries. This structural evolution is characteristic for the grain boundary sliding mechanism, when cavities grow to accommodate the strains induced at the grain boundaries. This further indicates on the lack of sufficient diffusional accommodating processes. The grain size effect, hence the grain boundary contribution to the plastic deformation may be manifested by Fig. 7, where the yield stress for polycrystalline Y_2O_3 with different grain size and at different strain rates versus the temperature is presented.[18,19,26] The strain rates in these investigations were $10^{-8}\,s^{-1}$ for the single crystals,[26] and varied between 5.7×10^{-6} and $10^{-5}\,s^{-1}$ for the polycrystalline specimens, by which the yield stress was determined. The brittle to ductile transition (BDT) temperature in pure polycrystalline Y_2O_3 with 600 nm grains decreased with the strain rate decrease; the lowest BDT of 1200 °C was at the strain rate of $10^{-7}\,s^{-1}$.[18] Our results for nanocrystalline Y_2O_3 in Fig. 7 verify the consistent effect of the grain boundaries on the onset temperature for plastic deformation; the BDT temperature decreased to ~1000 °C with decrease in the grain size into the nanometer size range (i.e. 110 nm).

In order to verify the contribution of the grain size and the grain boundaries to the observed plastic deformation, one should refer to the well documented literature on the plastic deformation of Y_2O_3. Following the plastic deformation mechanisms reported for Y_2O_3 single crystals, dislocation climb and glide were proved to dominate at the lower and the higher stresses, respectively, above 1200 °C ($0.54\,T_m$, the oxide melting point).[16,19,26] Strong dynamic grain growth at temperatures above 1400 °C was reported in polycrystalline Y_2O_3.[18,20] This dynamic grain growth, where the grains grew 3–6 times larger during the deformation, was related to the observed hardening effect. Significant grain growth was also observed during the densification of pure nanocrystalline Y_2O_3 by SPS above 1200 °C to the micrometer size range.[27] However, plastic deformation in the present study was tested at relatively lower temperatures (1050–1100 °C). Strain hardening appeared by decreasing the temperature by 50 °C and disappeared by increasing the temperature by 50 °C (Fig. 3). Consequently, this observed hardening cannot be accounted for the dynamic grain growth, as this process is faster at higher temperature. Instead, increasing the temperature is expected to enhance grain boundary diffusion at these temperatures, hence enhance the grain boundary accommodation processes. Therefore, deformation by grain boundary sliding is the most plausible mechanism in the present nanocrystalline specimens and supported by the nanostructure evolution.

The calculated activation energies of $440 \pm 70\,kJ\,mol^{-1}$ can be compared to those for various diffusional processes from the literature.[27–29] The measured activation energy is close to the value $410\,kJ\,mol^{-1}$ measured for grain boundary diffusion of Y^{3+} cation in nanocrystalline Y_2O_3.[29] The measured activation energies ~320–386 $kJ\,mol^{-1}$ reported for the plastic flow at higher temperatures,[18,26] where significant elongation of the grains were recorded. These latter activation energies refer most probably to diffusion of Y^{3+} cation within the lattice for

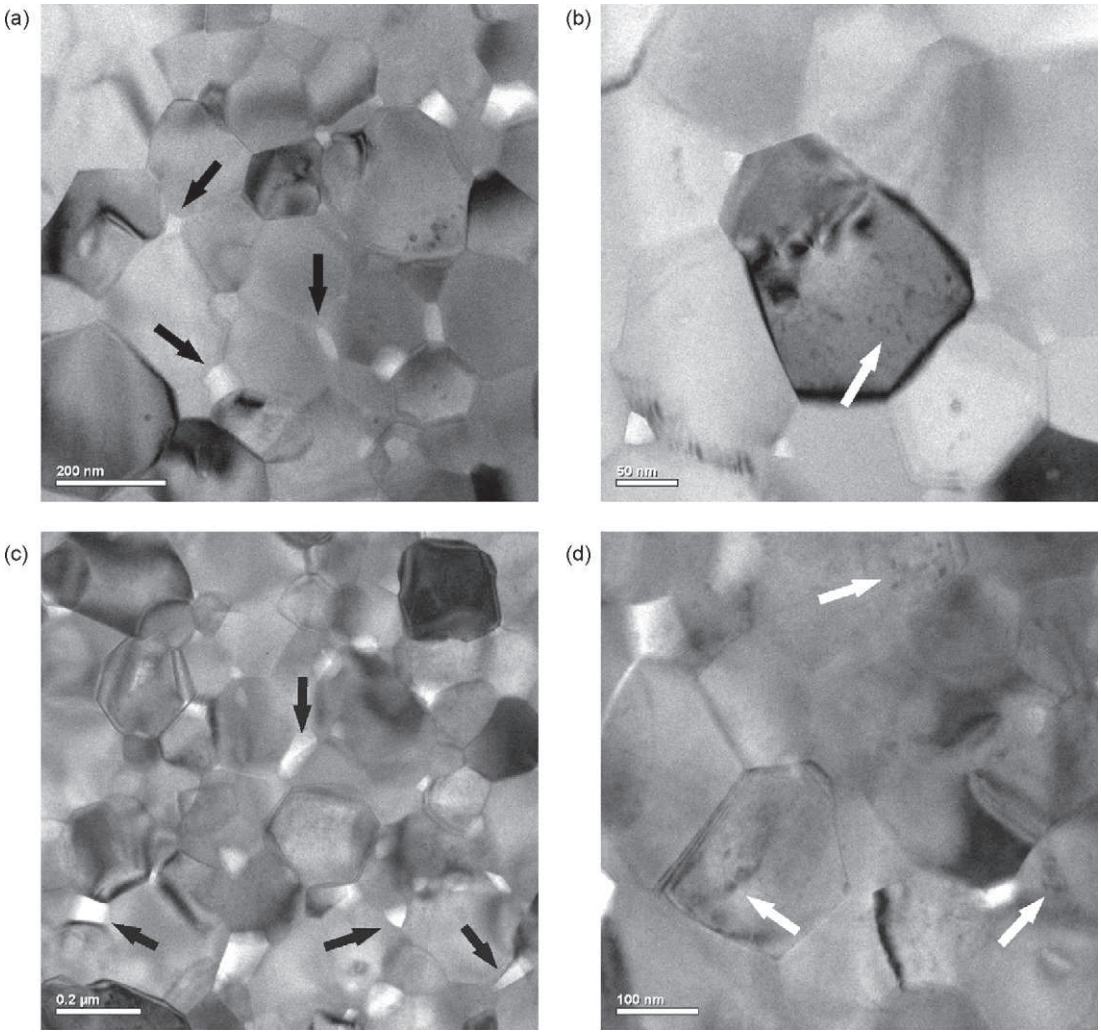

Fig. 6. TEM images from the deformed nc-Y_2O_3 specimens. (a and b) Interrupted creep in Ar (specimen in Fig. 2). (c and d) Deformed in air at constant strain rate to 29% strain (specimen in Fig. 3). The equiaxed shape of the grains is preserved. The arrowed nano-pores in (a and c) accommodate the strains at the gb and are characteristic for the grain boundary sliding mechanism. Dislocation loops arrowed in (b and d), visible in almost all grains under dynamic diffracting conditions, indicate very slow lattice diffusion.

dislocation climb.[27,30] On the other hand, the stacking fault energy in Y_2O_3 was calculated to be relatively low $\sim$80 J m^{-2}.[16] The fact that small dislocation loops were observed within the grains is compatible with formation of such stacking faults, bounded by partial dislocations.[26] This is a manifestation of the very slow lattice diffusion within the grains where cation vacancies remain within the grains. In parallel, the grain boundaries act as sinks for the vacancies formed at the grain boundary mantle; the resultant deformation rate controlling mechanism is then cation diffusion along the grain boundaries assisting the grain boundary sliding.

The stress exponent value of 2.0 ± 0.3 agrees with some of the uncorrected values reported for sub-micrometer size polycrystalline Y_2O_3 deformed in tension at 1400–1550 °C with strain-rates similar to our experiments.[18] Decrease in the value of the stress exponent from 2 to 1 is expected as the grain size increases, as stated when deformation by grain-boundary sliding via pure-shear motion is accommodated by lattice or grain-boundary diffusion.[31] In this respect, we can estimate the parameter β which quantifies the relative contributions of diffusion (motion perpendicular to the gb, with a characteristic time $\delta\tau_D$) and shear (motion parallel to the gb, with a characteristic time $\delta\tau_S$) to plastic deformation. The β parameter is defined as[31]:

$$\beta = \frac{\delta\tau_S}{\delta\tau_D} = \frac{3\pi}{4}\frac{\delta\sigma}{\gamma}\frac{\pi\delta}{d} \tag{2}$$

where δ is the thickness of gb diffusion layer ($\sim$0.4 nm), σ is the effective stress (applied stress or yield stress $\sim$150 MPa), γ is the grain boundary energy, estimated for yttria as 0.83 J m^{-2} [32] and d is the grain size, taken as 110 nm.

The β parameter has a direct influence on the stress exponent according to[31]:

$$n = \frac{2}{1+\beta} \tag{3}$$

Therefore, the stress exponent tends to $n = 2$ when β is small, to say the shear contribution by diffusion along the

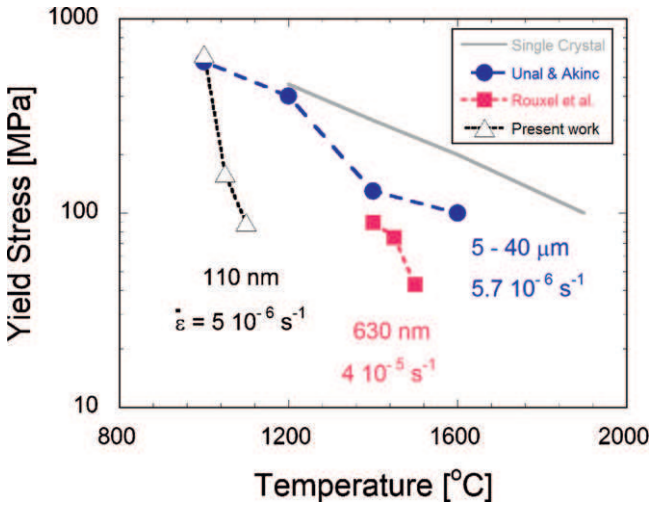

Fig. 7. Yield stress versus temperature for single crystal (solid line) and polycrystalline Y_2O_3 with different grain size. The grain size and corresponding strain rates for each test were indicated. The effect of the grain boundaries in the nanometer range on decrease of the onset temperature for plasticity is visible.

grain boundaries is much faster than diffusion perpendicular to the gb, into the grain bulk, and tends to 1 when the characteristic times for shear and diffusion become comparable.

Substitution of the above data for the present nanocrystalline Y_2O_3 in Eqs. (2) and (3) results in values of $\beta = 0.00194$ and $n = 1.99$. These theoretical expectations are in good agreement with the measured stress exponent value. This may additionally confirm the significant contribution of the gb processes to the plastic deformation in nanocrystalline Y_2O_3 at lower temperatures.

5. Summary and conclusions

Nanocrystalline Y_2O_3 with 110 nm average grain diameter was plastically deformed by compression at constant strain rate and creep tests at different stresses between 800 °C and 1100 °C. Yield stress was strongly temperature dependent and the strain hardening almost disappeared at 1100 °C. The deformed grains grew but preserved their original equiaxed morphology, while the nano-pores grew and extended from the grain corners along the grain boundaries. Microstructure analyses of the deformed specimens was consistent with the stress exponent $n = 2$ measured experimentally and calculated theoretically for grain boundary sliding. The calculated activation energy was in agreement with diffusion of Y^{3+} along the grain boundaries. Consistent with the literature data, the decrease in the grain size led to decrease in the brittle to ductile transition temperature.

Acknowledgments

The financial support by the Spanish Ministry of Science and Innovation (MAT2009-11078) and by the Israel Ministry of Science is gratefully acknowledged.

References

1. Shen Z, Johnsson M, Zhao Z, Nygren M. Spark plasma sintering of alumina. *J Am Ceram Soc* 2002;**85**:1921–7.
2. Chaim R, Shen Z, Nygren M. Transparent nanocrystalline MgO by rapid and low-temperature spark plasma sintering. *J Mater Res* 2004;**19**: 2527–31.
3. Anselmi-Tamburini U, Garay JE, Munir ZA. Fast low-temperature consolidation of bulk nanometric ceramic materials. *Scripta Mater* 2006;**54**: 823–8.
4. Chaim R, Reinharz Bar-Hama O. Densification of nanocrystalline NiO ceramics by spark plasma sintering. *Mater Sci Eng A* 2010;**527**:462–8.
5. Kim BN, Hiraga K, Morita K, Sakka Y. A high-strain-rate superplastic ceramic. *Nature* 2001;**413**:288–91.
6. Yoshida M, Shinoda Y, Akatsu T, Wakai F. Superplasticity-like deformation of nanocrystalline monoclinic zirconia at elevated temperatures. *J Am Ceram Soc* 2004;**87**:1122–5.
7. Gutierrez-Mora F, Dominguez-Rodriguez A, Jimenez-Melendo M, Chaim R, Hefetz M. Creep of nanocrystalline Y-SZP ceramics. *Nanostruct Mater* 1999;**11**:531–7.
8. Roddy MJ, Cannon WR, Skandan G, Hahn H. Creep behavior of nanocrystalline monoclinic ZrO_2. *J Eur Ceram Soc* 2002;**22**:2657–62.
9. Dominguez-Rodriguez A, Gomez-Garcia D, Zapata-Solvas E, Shen JZ, Chaim R. Making ceramics ductile at low homologous temperatures. *Scripta Mater* 2007;**56**:89–91.
10. Morita K, Hiraga K. Critical assessment of high-temperature deformation and deformed microstructure in high-purity tetragonal zirconia containing 3 mol% yttria. *Acta Mater* 2002;**50**:1075–85.
11. Dominguez-Rodriguez A, Gomez-Garcia D, Castillo-Rodriguez M. A critical assessment of the dislocation-driven model for superplasticity in yttria tetragonal zirconia polycrystals. *J Eur Ceram Soc* 2008;**28**:571–5.
12. Dominguez-Rodriguez A, Gomez-Garcia D, Castillo-Rodriguez M, Zapata-Solvas E, Chaim R. Superplasticity in nanocrystalline ceramics: pure grain boundary phenomena or not? *Int J Mater Res* 2010;**101**:1215–21.
13. Gutkin MY, Ovid'ko IA. Homogeneous nucleation of dislocation loops in nanocrystalline metals and ceramics. *Acta Mater* 2008;**56**:1642–9.
14. Chokshi AH. Unusual stress and grain size dependence for creep in nanocrystalline materials. *Scripta Mater* 2009;**61**:96–9.
15. Gaboriaud RJ, Veyssiere P, Rabier J, Boisson M. Plasticity of monocrystalline yttrium oxide (Y_2O_3) at 0.45 T_m. *J Mater Sci* 1978;**13** [Letters 907-08].
16. Gaboriaud RJ, Boisson M. Dissociation of the dislocation and plasticity of the yttrium sesquioxyde: Y_2O_3. *J Phys C* 1980;**6**:171–4.
17. Akcurin MS, Zakalyukin RM, Kovalchuk MV, Kupenko II. Mechanical twinning of yttrium oxide single crystals. *J Surf Invest (X-ray, Sync, Neut Tech)* 2010;**4**:923–7.
18. Rouxel T, Murat D, Besson JL, Boncoeur M. Large tensile ductility of high purity polycrystalline yttria. *Acta Mater* 1996;**44**:263–78.
19. Ünal Ö, Akinc M. Compressive properties of yttrium oxide. *J Am Ceram Soc* 1996;**79**:805–8.
20. Besson JL, Murat D, Rouxel T, Valin F, Boncoeur M. Compressive creep of a fine-grained polycrystalline yttria. *J Am Ceram Soc* 1996;**79**:773–6.
21. Yoshida H, Morita K, Kim BN, Hiraga K, Kodo M, Soga K, et al. Densification of nanocrystalline yttria by low temperature spark plasma sintering. *J Am Ceram Soc* 2008;**91**:1707–10.
22. Marder R, Chaim R, Estournès C. Grain growth stagnation in fully dense nanocrystalline Y_2O_3 by spark plasma sintering. *Mater Sci Eng A* 2010;**527**:1577–85.
23. Yoshida H, Morita K, Kim BN, Hiraga K, Yamanaka K, Soga K, et al. Low-temperature spark plasma sintering of yttria ceramics with ultrafine grain size. *J Am Ceram Soc* 2011;**94**:3301–7.
24. Gervais H, Pellicier BY, Castaing J. Creep machine for high-temperature compression tests of ceramics. *Rev Int Hautes Temp Réfract* 1978;**15**:43–7.
25. Bravo-León A, Jiménez-Melendo M, Domínguez-Rodríguez A, Chokshi AH. *J Mater Sci Lett* 1994;**13**:1169–70.
26. Gaboriaud RJ. High-temperature creep of yttrium sesquioxyde: Y_2O_3. *Philos Mag A* 1981;**44**:561–87 [in French].

27. Chaim R, Shlayer A, Estournès C. Densification of nanocrystalline Y_2O_3 ceramic powder by spark plasma sintering. *J Eur Ceram Soc* 2009;**29**:91–8.
28. Chen PL, Chen IW. Grain boundary mobility in Y_2O_3. *J Am Ceram Soc* 1996;**79**:1801–9.
29. Wang XH, Chen PL, Chen IW. Two-step sintering of ceramics with constant grain size, I. Y_2O_3. *J Am Ceram Soc* 2006;**89**: 431–7.
30. Gaboriaud RJ. Self-diffusion of yttrium in monocrystalline yttrium oxide: Y_2O_3. *J Solid State Chem* 1980;**35**:252–61.
31. Gómez-García D, Zapata-Solvas E, Domínguez-Rodríguez A, Kubin LP. Diffusion-driven superplasticity in ceramics: modeling and comparison with available data. *Phys Rev B* 2009;**80**:214107.
32. Zhang P, Navrotsky A, Guo B, Kennedy I, Clark AN, Lesher C, et al. Energetics of cubic and monoclinic yttrium oxide polymorphys: phase transitions, surface enthalpies, and stability at the nanoscale. *J Phys Chem C* 2008;**112**:932–8.